Pleistocene Sunda Shelf submersion-exposure cycles initiate vegetation Walker Circulation feedback

Sarah M. McGrath*, Steven C. Clemens, and Yongsong Huang

Earth, Environmental, and Planetary Sciences, Brown University, Providence, Rhode Island 02912, USA

ABSTRACT

Recent research has found that the subsiding Sunda Shelf (Southeast Asia) was permanently exposed prior to ca. 400 ka with initial submersion-exposure cyclicity, associated with interglacial-glacial sea-level cycles, beginning between 400 and 240 ka. We analyzed the impact submersion-exposure cycles on regional environment and climate through a 640 k.y. leaf-wax carbon isotope ($\delta^{13}C_{wax}$) reconstruction at Andaman Sea Site U1448, representing relative changes in C_3/C_4 plant abundances. Prior to ca. 250 ka, the Sunda region was inhabited by a stable C_3 (forest) biome, after which submersion-exposure cycles initiated with the deglacial sea-level rise at ca. 250 ka. During subsequent glacial-age sea-level drops, the newly exposed shelf was rapidly colonized by C_4 grasses, followed by slow transitions back to C_3 forests, representing a tenfold increase in the variability of C_3/C_4 vegetation in the Sunda region. The C_3/C_4 regime shift since 250 ka is coherent across the Southeast (SE) Asia peninsula and Sunda Shelf and is coincident with a shift in the east-west sea-surface temperature gradient in the equatorial Pacific Ocean. We hypothesize that the expansion of C_4 grasslands promoted and sustained drier glacial-age climates over SE Asia via a feedback mechanism that contributed to weakening the ascending branch of the east-west atmospheric circulation in the equatorial Pacific region known as the Walker Circulation. Our results indicate that the Sunda Shelf region has a larger influence on Walker Circulation than is seen in current paleoclimate simulations.

INTRODUCTION

Southeast Asia is a key component of the tropical climate system, characterized by deep convection associated with the ascending branch of Walker Circulation (east-west atmospheric circulation in the equatorial Pacific Ocean). The modern Sunda Shelf (Fig. 1) is on average ~50 m deep (Sarr et al., 2019a). During the late Pleistocene, submersion-exposure cycles initiated such that the shelf was submerged during interglacials and exposed during glacials. Modeling efforts show that Sunda, Sahul, and northwestern Australia shelf exposure influence Walker Circulation to varying degrees, resulting in drier conditions over the eastern Indian Ocean and SE Asia and wetter conditions over the western Indian Ocean (DiNezio and Tierney, 2013; DiNezio et al., 2016, 2018; Du et al., 2021).

Submersion rates indicate the Sunda Shelf was permanently exposed prior to 400 ka, and may have been permanently exposed until ca. 240 ka (Sarr et al., 2019a). The environmental and climate impacts of the transition from a permanently exposed Sundaland to an interglacial submerged and glacially exposed Sunda Shelf are under-constrained. We assess the coupled vegetation-climate responses to Sunda Shelf submersion-exposure cycles based on 640 k.y. reconstructions of SE Asian vegetation using organic biomarker and stable isotopic proxies. We find that the submersion of the shelf perturbed an otherwise stable C_3 forest biome, creating interglacial-glacial variability beginning at 250 ka. Prior to 250 ka, interglacial-glacial variability had a muted impact on the vegetation structure of the Sunda region. Our reconstructions indicate the initiation of Sunda Shelf submersion-exposure cycles resulted in a regime shift during glacials when C_4 grassland expansion promoted drier regional conditions,

and contributed to weakened Walker Circulation across the Indo-Pacific region.

VEGETATION SHIFTS
Leaf-Wax Vegetation Proxies

To reconstruct vegetation, we analyzed leaf waxes from Integrated Ocean Drilling Program (IODP) Andaman Sea Site U1448 (Fig. 1; Figs. S1 and S2 in the Supplemental Material[1]). The $\delta^{13}C$ of C_{26}, C_{28}, C_{30}, and C_{32} alkanoic acids exhibit the same structure, with higher chain lengths showing larger isotopic changes relative to smaller chain lengths (Fig. 2B). The $\delta^{13}C$ values of C_{30} and C_{32} are on average 3.5‰ depleted compared to those of C_{26} and C_{28}, except for the last two glaciations when all values converge. The average leaf wax carbon isotope ($\delta^{13}C_{wax}$) value of the n-alkanoic acids was calculated by averaging the $\delta^{13}C$ of C_{26}, C_{28}, C_{30}, and C_{32}. The $\delta^{13}C_{wax}$ record shows ^{13}C-enriched values during glacial periods and ^{13}C-depleted values during interglacial periods. The n-alkanes average chain length record (Fig. 2A) shows larger values during glacials and smaller values during interglacials.

From 640 to 250 ka, Site U1448 vegetation proxies suggest a stable SE Asian vegetation structure. The $\delta^{13}C_{wax}$ variability exhibits a muted 0.3‰ range over interglacial-glacial cycles. The average chain length signal is very stable, with an average of 30.5 ± 0.1 (1 standard deviation [s.d.]). Prior to 250 ka, the interglacial-glacial range of the $\delta^{13}C_{wax}$ records indicates mild C_4 expansion during glacials.

After 250 ka, interglacial-glacial variability increases in both $\delta^{13}C_{wax}$ and average chain length, with average $\delta^{13}C_{wax}$ increasing by 10 times, to 3‰. This post–250 ka amplification is present in all n-fatty acids with $\delta^{13}C$, C_{30}, and C_{32} records exhibiting twice the amplitude of interglacial-glacial change relative to that of $\delta^{13}C$, C_{26}, and C_{28}. Glacial-age average chain length

Sarah M. McGrath [iD] https://orcid.org/0000-0003-3372-1894

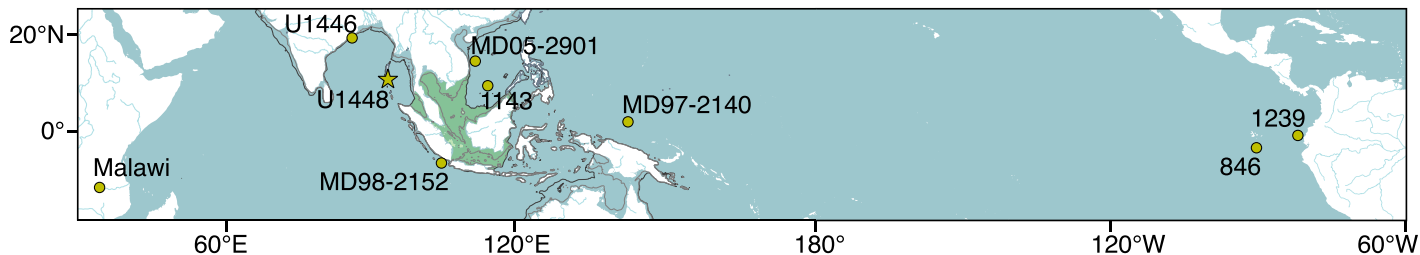*Current affiliation: Abt Associates, sarah_mcgrath@abtassoc.com

Figure 1. Site location map. Gray and black lines indicate the 40 m and 120 m isobaths, respectively.

decreases to 30.1 ± 0.3 (1 s.d.), and a minimum of 29.2. While post–250 ka interglacial $\delta^{13}C_{wax}$ values rebound back to pre–250 ka values, the post–250 ka interglacial average chain length rebounds to values 0.5 shorter than the pre–250 ka values, with shortest average chain length during the Holocene. Over the past 250 k.y., glacial periods have longer average chain length, and interglacial periods have shorter average chain length. The longer average chain length during glacials suggest C_4 and grass expansion over C_3 trees, as tropical grasses have greater chain lengths than trees (i.e., Vogts et al., 2009). The post–250 ka changes in both $\delta^{13}C_{wax}$ and average chain length support widespread C_4 grass expansion during glacials.

Overall, the Site U1448 vegetation proxies indicate a relatively stable C_3 (forest-dominated) vegetation from 640 ka until the shift at ca. 250 ka, followed by enhanced interglacial-glacial variability characterized by expansion of C_4 grasses onto newly exposed shelf during

sea-level regression, followed by a slow transition back to C_3 (forest-dominated) vegetation (Fig. 2). An average Sunda Shelf subsidence rate of between 0.2 mm/yr and 0.3 mm/yr (Sarr et al., 2019a; Salles et al., 2021) is consistent with the large vegetation shifts being influenced by Sunda Shelf submersion beginning at 250 ka (Fig. 2F). We note that the Site U1448 $\delta^{13}C_{wax}$ does exhibit a minor 2‰ shift in C_3 and C_4 proportions at 360 ka, during the glacial Marine Isotope Stage (MIS) 10 interval, suggesting a brief submersion during MIS 11 (ca. 400 ka). After 250 ka, there are substantial shifts in C_3 and C_4 proportions, corresponding to the larger and longer submersion during MIS 9 and thereafter.

Interglacial-Glacial Regional Carbon Isotopes Patterns

The Andaman Site U1448 $\delta^{13}C_{wax}$ record has a very different signal compared to that of Site U1446 (Figs. 1 and 2D). Indian margin Site U1446 captures terrestrial sediment from

the core monsoon zone of India, including the Mahanadi River Basin and drainages to the north (Ganges and Brahmaputra). The differences in the U1446 and U1448 $\delta^{13}C_{wax}$ structure indicates that vegetation input to these sites has different forcing mechanisms; CO_2 is the predominant factor driving interglacial-glacial variability in U1446 $\delta^{13}C_{wax}$ (Yamamoto et al., 2022). The evolutionary power spectrum of U1446 $\delta^{13}C_{wax}$ (Fig. S3A) shows strong 100 k.y. power throughout the record, with the strongest power between 500 ka and 300 ka. The evolutionary power spectrum of U1448 $\delta^{13}C_{wax}$ differs (Fig. S3B), with the strongest 100 k.y. power after 250 ka. The U1446 and U1448 $\delta^{13}C_{wax}$ records are only weakly coherent (Fig. S4A) indicating that vegetation input to the Andaman region is less sensitive to global-scale CO_2, and instead more sensitive to slow tectonic subsidence coupled with regional sea level and climate shifts.

While the U1446 and U1448 $\delta^{13}C_{wax}$ records have different structure, the U1448 $\delta^{13}C_{wax}$ record is very similar to that of the tropical Indian Ocean core MD98-2152 (MD111 leg of the IMAGES IV Cruise) $\delta^{13}C_{wax}$ record, located on the southern Sumatran margin (Figs. 1 and 2C). The MD98-2152 record captures the terrestrial signal from the Sumatra and Java islands and shows increasing glacial variability over the last two glacial periods (Windler et al., 2019) with less interglacial-glacial variability between 450 ka to 250 ka; very similar to the U1448 $\delta^{13}C_{wax}$ record (Figs. 2C and 3A; Fig. S3C). Both $\delta^{13}C_{wax}$ records fall within the large-range discrete $\delta^{13}C$ of SE Asian mammal teeth from the mid-Pleistocene to Holocene (Louys and Roberts, 2020).

Windler et al. (2019) interpreted the glacial amplification in the $\delta^{13}C_{wax}$ as resulting from global sea level influencing Sunda Shelf exposure during the last two glacial periods. If global sea level and Sunda Shelf exposure alone were the primary driving factors for $\delta^{13}C_{wax}$ glacial variability at Site U1448, then according to the global sea-level curves (Spratt and Lisiecki, 2016), $\delta^{13}C_{wax}$ should approach −24‰ during glacial MIS 12 (478–424 k.y.) and MIS 16 (676–621 k.y.) (Fig. 2B). The lack of large interglacial-glacial $\delta^{13}C_{wax}$ variability at these times in the extended Site U1448 record supports the combination of subsidence and global sea-level variability as the drivers of the post–
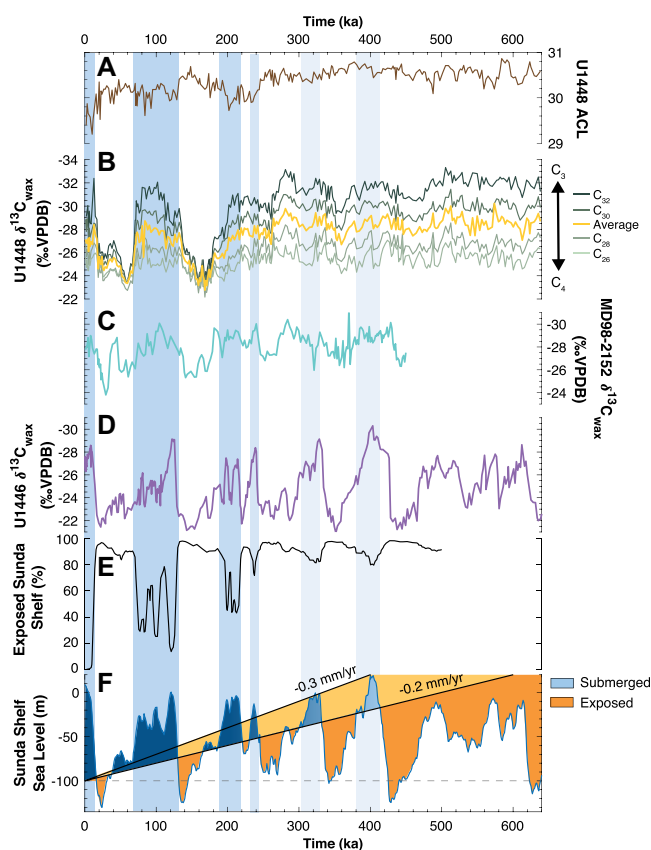

Figure 2. Vegetation proxies and Sunda Shelf (Southeast Asia) exposure. (A) Integrated Ocean Drilling Program (IODP) Site U1448 *n*-alkane average chain length (ACL). (B) Site U1448 leaf-wax carbon isotope ($\delta^{13}C_{wax}$) values. (C) Sediment core MD98-2152 (MD111 leg of the IMAGES IV Cruise) $\delta^{13}C_{wax}$ (Windler et al., 2019). (D) IODP Site U1446 $\delta^{13}C_{wax}$ (Yamamoto et al., 2022). (E) Percent Sunda Shelf exposure (Salles et al., 2021). (F) Global sea-level curve (Spratt and Lisiecki, 2016), with black lines showing Sunda Shelf subsidence rates (Sarr et al., 2019a) and gray dashed line showing shelf exposure in the absence of subsidence. Site and core locations are shown in Figure 1. VPDB—Vienna Peedee belemnite.
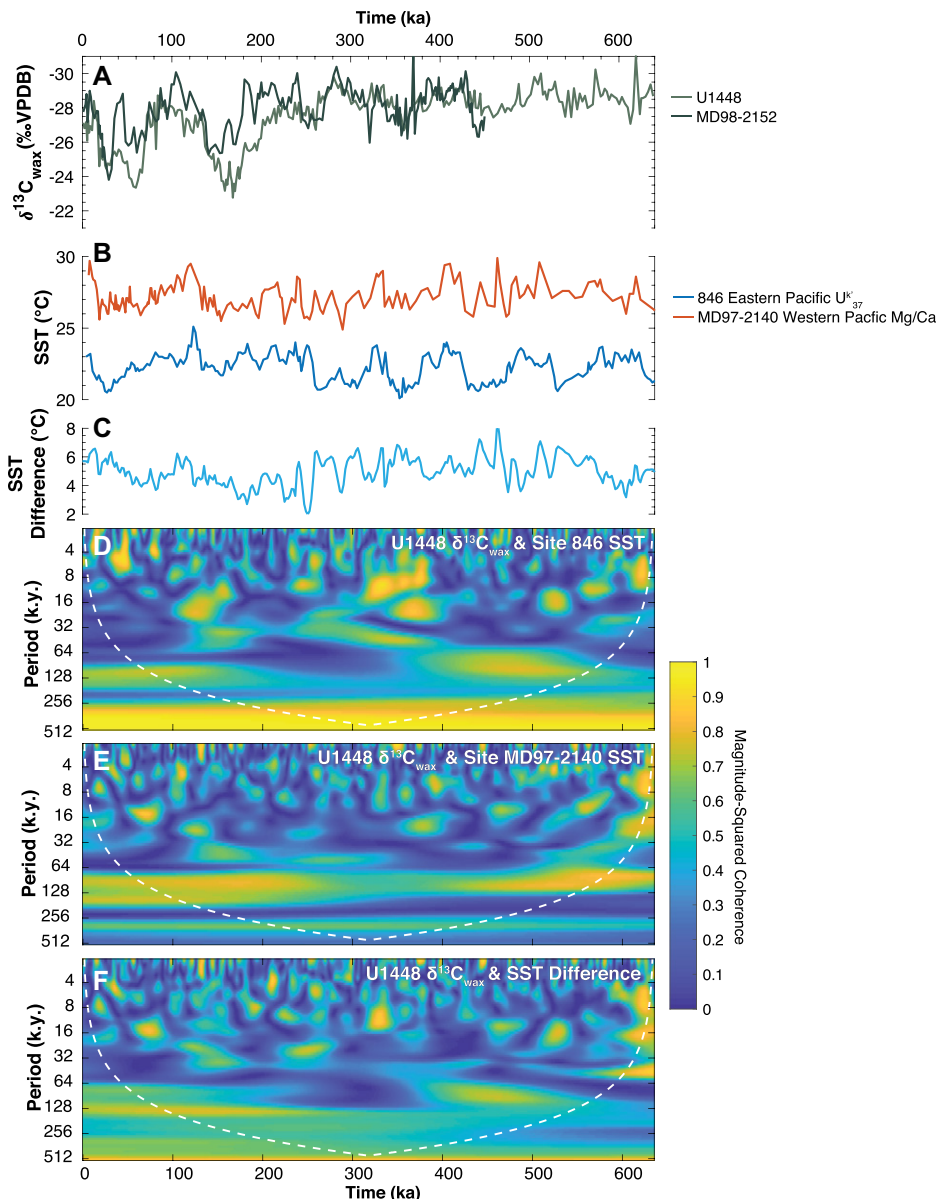
Figure 3. Southeast Asia (SE) vegetation relationship with the Pacific Ocean sea-surface temperature (SST) gradient. (A) SE Asia leaf-wax carbon isotope ($\delta^{13}C_{wax}$) values. (B) Pacific SSTs (Liu and Herbert, 2004; De Garidel-Thoron et al., 2005). (C) El Niño–Southern Oscillation (ENSO) proxy by SST difference of the western Pacific warm pool (IMAGES core MD97-2140) and Eastern equatorial Pacific (Ocean Drilling Program [ODP] Site 836). (D–F) Wavelet cross-spectra of Integrated Ocean Drilling Program (IODP) Site U1448 $\delta^{13}C_{wax}$ and SST records. Site and core locations are shown in Figure 1. VPDB—Vienna Peedee belemnite.

250 ka glacial C_4 expansions across SE Asia and the Sunda Shelf.

WALKER CIRCULATION CHANGE

Existing models indicate that shelf exposure should be the largest influence on regional atmospheric circulation, although they diverge regarding the relative influence of the different shelf regions and the influence of changing vegetation. Sarr et al. (2019b) found that, secondary to land exposure, vegetated surface properties modulate the radiative effect and turbulent heat flux. Expanded C_4 grasslands produced weaker evaporation rates, lower latent heat release, and less surface cooling than a C_3 rainforest, leading toward less precipitation in the Sunda Shelf region (Sarr et al., 2019b). DiNezio et al. (2016) prescribed widespread C_4 grasses to represent the vegetation of the Sunda and Sahul shelves, and found vegetation was not a first-order influence on the atmospheric responses to shelf exposure. They found similar responses in the Walker Circulation, albeit of slightly different magnitude, for unvegetated and vegetated conditions. DiNezio et al. (2016) found that most of the simulated drying over the Sunda Shelf is caused by exposure of the Sahul Shelf. Within the model, the Sahul Shelf has a larger influence

than the Sunda Shelf on regional Indo-Pacific Walker Circulation (DiNezio et al., 2016, 2018). Du et al. (2021) did not test for the impact of vegetation changes on exposed shelves but did find that exposure of the northwestern Australian shelf excited a Bjerknes feedback across the equatorial Indian Ocean, driving decreased Walker Circulation, a result that was not evident with exposure of the Sunda or Sahel shelves.

In contrast to these model results, proxy records point to the Sunda Shelf submersion-exposure cycles and consequent changes in vegetation as a significant driver of Indo-Pacific Walker Circulation change. The vegetation and sea-surface temperature (SST) proxy records show that glacials experienced the largest changes after initiation of the Sunda Shelf interglacial-glacial submersion-exposure cycles. We propose that the vegetation variability is driven by C_4 plants colonizing the exposed shelf and that the C_4 vegetation both promotes and helps sustain a drier climate through Walker Circulation feedbacks.

Pacific Walker Circulation

Proxy records show a change in interglacial-glacial variability of Pacific SST after 250 ka. The Western Pacific Warm Pool shows an amplification of interglacial-glacial SST difference post–250 ka (Fig. 3C). The eastern equatorial Pacific cold tongue shows a weakening of interglacial-glacial SST difference, with glacial SSTs becoming warmer post–250 ka (Fig. 3B). This suggests Pacific SSTs are also influenced by the initiation of the Sunda Shelf submersion-exposure cycles.

Southeast Asia vegetation records have statistically significant spectral coherence with Pacific SSTs. There is high coherence of SE Asia $\delta^{13}C_{wax}$ with warm pool SST at the 100 k.y. interglacial-glacial period, with warm SSTs associated with C_3 abundance (Fig. 3E). Post–250 ka, the cooler glacial warm pool SSTs and C_4 expansion would both drive a weaker Pacific Ocean Walker Circulation through weakening the ascending branch over SE Asia (Fig. 4B). Southeast Asia $\delta^{13}C_{wax}$ records also show high coherence with eastern equatorial Pacific cold tongue SST at the 100 k.y. interglacial-glacial period prior to 250 ka (Fig. 3D). Post–250 ka, there is a shift in cold tongue SST (Liu and Herbert, 2004; Etourneau et al., 2010) as SST remains warmer during glacials over the past 250 k.y. (Fig. 3B). A warmer cold tongue SST would weaken the descending branch of Pacific Ocean Walker Circulation over the eastern equatorial Pacific.

The SST difference between the western Pacific warm pool core MD97-2140 (De Garidel-Thoron et al., 2005) and the eastern equatorial Pacific cold tongue Ocean Drilling Program (ODP) Site 846 (Fig. 1; Liu and Herbert, 2004) has been used as an El Niño–South-
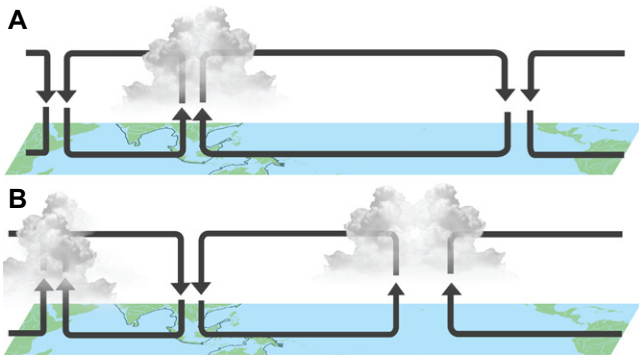
Figure 4. Schematic of the Indo-Pacific Walker Circulation change. Conditions when (A) C_3 plants dominate pre–250 ka glacials and all interglacials, and (B) C_4 plants dominate glacials after 250 ka.

ern Oscillation (ENSO) proxy (De Garidel-Thoron et al., 2005) with greater SST difference representing La Niña–like conditions (strong Pacific Walker Circulation), and smaller SST difference representing El Niño–like conditions (weak Pacific Walker Circulation). We note here that ENSO is a sub-decadal process; the "ENSO-like" conditions we refer to describe interglacial-glacial large-scale circulation patterns whereby the average background climate state tends toward stronger (La Niña) or weaker (El Niño) Walker circulation. At 250 ka, there is an inflection point in ENSO proxy representing a shift to more El Niño–like conditions thereafter (Fig. 3C). The SE Asian $\delta^{13}C_{wax}$ records are highly coherent over the past 250 k.y. with Pacific SSTs and the SST-based ENSO reconstruction, following modern trends (Figs. S4C–S4E; see the Supplemental Material). Thus, observations indicate a weakening of Pacific Ocean Walker Circulation during glacials post–250 ka (Fig. 3), coinciding with the initiation of the Sunda Shelf submersion-exposure cycles. We propose glacial-age Walker Circulation is further weakened through the Sunda Shelf vegetation feedback that initiates due to submersion-exposure cycles (Fig. 4).

Indian Walker Circulation

Observations have shown evidence of weakened Walker Circulation over the Indian Ocean post–250 ka. Windler et al. (2019) presented proxy and model evidence indicating that a cooling of the subsurface and shoaling of the thermocline in the eastern Indian Ocean drive a weakened glacial Indian Ocean Walker Circulation (Fig. S5). The weaker glacial Indian Ocean Walker Circulation creates drying over SE Asia and a wetting of eastern Africa (Windler et al. 2019). Proxies from Lake Malawi in eastern Africa show a wetter climate post–280 ka, with increased runoff and a shift to woodland vegetation (Johnson et al., 2016) (Fig. S5). Vegetation proxies across SE Asia show C_4 grassland expansion post–250 ka glacials is driven by expansion of C_4 plants on the exposed shelf. Sarr et al.'s (2019b) models indicate a C_4 grassland promotes a drier climate compared to that of

a C_3 forest. The SE Asia C_4 vegetation is both sustained by and promotes a drier climate.

CONCLUSIONS

The initiation of Sunda Shelf submersion-exposure cycles at 250 ka perturbed the otherwise stable C_3 (forest) vegetation biome that existed prior to that time, when the shelf region was subsiding, but not yet experiencing submersion-exposure cycles. After submersion, the subsequent exposure created land that was preferentially colonized by C_4 grasses. This biome further promoted drier conditions over SE Asia and weakening of ascending atmospheric motion with consequent weakening of the Indo-Pacific Walker Circulation. This is substantiated by the El Niño–like climate state inferred from equatorial Pacific SST gradient reconstructions. Across the Indian Ocean, there is evidence for a weaker glacial Indian Ocean Walker Circulation that also supports a drier maritime continent and SE Asia climate and a wetter eastern Africa climate. Thus, post–250 ka, there is a relationship between Sunda Shelf submersion-exposure cycles and vegetation feedbacks that promote enhanced Walker Circulation and climate variability across the Indo-Pacific region.

REFERENCES CITED

De Garidel-Thoron, T., Rosenthal, Y., Bassinot, F., and Beaufort, L., 2005, Stable sea surface temperatures in the western Pacific warm pool over the past 1.75 million years: Nature, v. 433, p. 294–298, https://doi.org/10.1038/nature03189.

DiNezio, P.N., and Tierney, J.E., 2013, The effect of sea level on glacial Indo-Pacific climate: Nature Geoscience, v. 6, p. 485–491, https://doi.org/10.1038/ngeo1823.

DiNezio, P.N., Timmermann, A., Tierney, J.E., Jin, F.F., Otto-Bliesner, B., Rosenbloom, N., Mapes, B., Neale, R., Ivanovic, R.F., and Montenegro, A.,

2016, The climate response of the Indo-Pacific warm pool to glacial sea level: Paleoceanography, v. 31, p. 866–894, https://doi.org/10.1002/2015PA002890.

DiNezio, P.N., Tierney, J.E., Otto-Bliesner, B.L., Timmermann, A., Bhattacharya, T., Rosenbloom, N., and Brady, E., 2018, Glacial changes in tropical climate amplified by the Indian Ocean: Science Advances, v. 4, https://doi.org/10.1126/sciadv.aat9658.

Du, X., et al., 2021, Deglacial trends in Indo-Pacific warm pool hydroclimate in an isotope-enabled Earth system model and implications for isotope-based paleoclimate reconstructions: Quaternary Science Reviews, v. 270, https://doi.org/10.1016/j.quascirev.2021.107188.

Etourneau, J., Schneider, R., Blanz, T., and Martinez, P., 2010, Intensification of the Walker and Hadley atmospheric circulations during the Pliocene–Pleistocene climate transition: Earth and Planetary Science Letters, v. 297, p. 103–110, https://doi.org/10.1016/j.epsl.2010.06.010.

Johnson, T.C., et al., 2016, A progressively wetter climate in southern East Africa over the past 1.3 million years: Nature, v. 537, p. 220–224, https://doi.org/10.1038/nature19065.

Liu, Z., and Herbert, T.O., 2004, High-latitude influence on the eastern equatorial Pacific climate in the early Pleistocene epoch: Nature, v. 427, p. 720–723, https://doi.org/10.1038/nature02338.

Louys, J., and Roberts, P., 2020, Environmental drivers of megafauna and hominin extinction in Southeast Asia: Nature, v. 586, p. 402–406, https://doi.org/10.1038/s41586-020-2810-y.

Salles, T., Mallard, C., Husson, L., Zahirovic, S., Sarr, A.C., and Sepulchre, P., 2021, Quaternary landscape dynamics boosted species dispersal across Southeast Asia: Communications Earth & Environment, v. 2, p. 240, https://doi.org/10.1038/s43247-021-00311-7.

Sarr, A.C., Husson, L., Sepulchre, P., Pastier, A.M., Pedoja, K., Elliot, M., Arias-Ruiz, C., Solihuddin, T., Aribowo, S., and Susilohadi, 2019a, Subsiding Sundaland: Geology, v. 47, p. 119–122, https://doi.org/10.1130/G45629.1.

Sarr, A.C., Sepulchre, P., and Husson, L., 2019b, Impact of the Sunda Shelf on the climate of the maritime continent: Journal of Geophysical Research: D, Atmospheres, v. 124, p. 2574–2588, https://doi.org/10.1029/2018JD029971.

Spratt, R.M., and Lisiecki, L.E., 2016, A Late Pleistocene sea level stack: Climate of the Past, v. 12, p. 1079–1092, https://doi.org/10.5194/cp-12-1079-2016.

Vogts, A., Moossen, H., Rommerskirchen, F., and Rullkötter, J., 2009, Distribution patterns and stable carbon isotopic composition of alkanes and alkan-1-ols from plant waxes of African rain forest and savanna C_3 species: Organic Geochemistry, v. 40, p. 1037–1054, https://doi.org/10.1016/j.orggeochem.2009.07.011.

Windler, G., Tierney, J.E., DiNezio, P.N., Gibson, K., and Thunell, R., 2019, Shelf exposure influence on Indo-Pacific Warm Pool climate for the last 450,000 years: Earth and Planetary Science Letters, v. 516, p. 66–76, https://doi.org/10.1016/j.epsl.2019.03.038.

Yamamoto, M., Clemens, S.C., Seki, O., Tsuchiya, Y., Huang, Y., O'ishi, R., and Abe-Ouchi, A., 2022, Increased interglacial atmospheric CO_2 levels followed the mid-Pleistocene Transition: Nature Geoscience, v. 15, p. 307–313, https://doi.org/10.1038/s41561-022-00918-1.

Printed in the USA